Image processing tools for better incorporation of 4D seismic data into reservoir models

Ratiba Derfoul, Sébastien da Veiga, Christian Gout, Carole Le Guyader, Elodie Tillier

Image processing tools for better incorporation of 4D seismic data into reservoir models

Ratiba Derfoul[a,b], Sebastien Da Veiga[a], Christian Gout[b], Carole Le Guyader[b], Elodie Tillier[c]

[a] *IFP Energies nouvelles, 1-4 avenue de Bois Préau, 92852 Rueil-Malmaison, France*
[b] *INSA de Rouen, Laboratoire de Mathématiques de l'INSA, Avenue de l'Université, 76801 Saint-Etienne-du-Rouvray Cedex, France*
[c] *CIRAD, UMR AMAP, TA-A51/PS2, Boulevard de la Lironde, 34398 Montpellier, Cedex 5, France*

Abstract

Reservoir engineers have to predict the behavior of a hydrocarbon reservoir by building a simulation model which can reproduce as best as possible the data collected on the field. These data fall into two types: static data, which are invariable in time, and dynamic data, which evolve according to fluid motions in the reservoir. In this paper, we focus on the integration of dynamic data related to 4D inverted seismic data. Such seismic data constitute an invaluable source of information on fluid displacement and geology over extensive areas of the reservoir. However, incorporating them in the reservoir model through a matching process is a challenging task. Classical formulations of the objective function, which computes the misfit between observed data and responses computed by the reservoir model, are not adapted to 4D inverted seismic data. For example, a least square based mismatch is not representative of the visual difference between two seismic images. In this paper, we define a new formulation of the objective function based on simplification of seismic data in order to extract relevant information. This simplification involves filtering and segmentation techniques, as well as image comparison methods rooted in image analysis, such as the local modified Haussdorff distance. We investigate the efficiency of such techniques in the context of seismic data, and illustrate their potential on a synthetic history matching reservoir example.

Keywords: History matching, filtering, segmentation, image comparison

1. Introduction

History matching is an inverse problem where some parameters are modified in order to build a reliable reservoir model which can reproduce the field observed data. These data fall into two types: static data, which are invariable in time, and dynamic data, which evolve in time according to fluids motion in the reservoir. Traditionally, dynamic data consist of production data collected at wells. Nowadays, an other type of data called time-lapse seismic data can be acquired. These data are generated by using vibrations to capture a two-dimensional picture of rock layers beneath the surface at the same localisation but at different times. These data constitute a highly informative spatial information. The geologists interpret these data to make an estimated picture which can reveal the hydrocarbon motion under the surface without drilling.
Incorporating such data in a reservoir model calls for a specific workflow, which consists of a

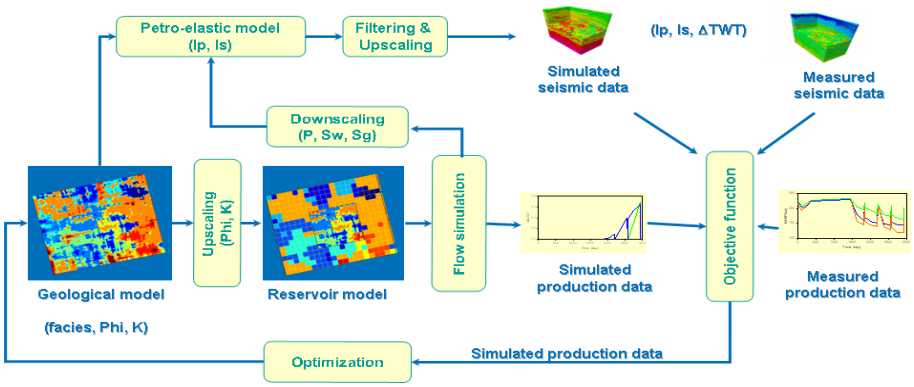

Figure 1: Illustration of the history matching loop.

chain of successive modelling steps. First, a geological model is built and populated with petrophysical properties such as porosity and permeability. Then, this model is upscaled to a reservoir grid used to perform a fluid flow simulation by resolving an hyperbolic equation system [3]. The result of these equations provides some simulated production data. Seismic attribute variations (velocity and acoustic impedances) can be derived from the computed pressure and saturation variations through a petro-elastic modeling. Typically, it involves linear equations called the Gassmann equations [16] to model fluid effects and the Hertz-Mindlin equations [19] to model pressure effects. Outputs of the petro-elastic model are then usually filtered for consistency with the typical seismic bandwidth. The resulting seismic attribute variations are called the simulated seismic attributes. Finally, comparison between simulated and observed data is performed through the evaluation of a so-called objective function. This objective function measures the misfit between available data and data simulated by a given reservoir model. Figure 1 summarizes the workflow used to build a reservoir model.

The history matching process is thus an inverse problem where an optimisation method is used to adjust the unknown parameters in order to reduce the value of the objective function. If the formulation of the objective function is adapted, at the end of the process the simulated data produced by the matched model will be close to the available data. Consequently, the definition of the objective function is crucial for this workflow. Currently, the objective function is based on a least square formulation, denoted by OF_{LS} and given by :

$$OF_{LS} = \frac{1}{2}(d - d^s)^t C^{-1}(d - d^s)$$

where d is the reference data vector, d^s is the simulated data vector and C is the covariance matrix, which represents the measurement uncertainties. This formulation encompasses both production and seismic data: as a result, all data are treated the same way. This formulation proved to be efficient for production data, in the sense that it is a good characterization of the error between simulated and real data. Moreover, during the history matching process, the objective function can be reduced significantly. On the contrary, this formulation is not suitable for seismic data. Indeed, the nature of inverted seismic data is totally different from production data. First, production data are few and are represented by curves, whereas seismic data are millions of points in a 3D cube with spatial information. Second, while the production data collected on the field are spoiled only by measurement errors, the available seismic attributes, such

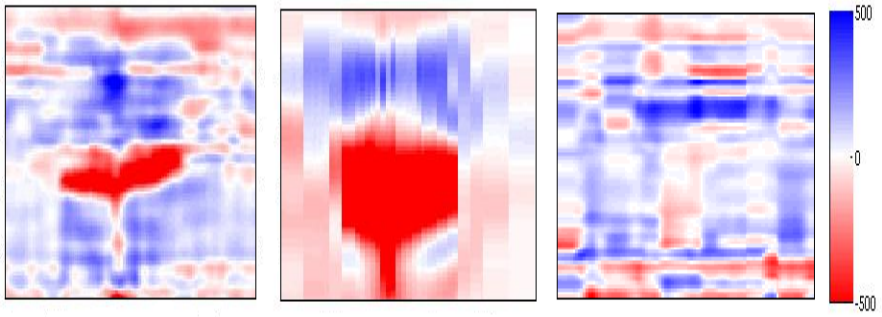

Figure 2: Least square formulation for seismic data. Reference (left), simulated (middle) and non-informative map (right). The value of the objective function between the reference and the simulation is 341, while it is about 120 between the reference and the non-informative map.

as P-impedances, have two types of incertitudes. Besides measurement errors observed during the seismic survey, additional uncertainty comes from the inversion process, which transforms a seismic reflection data into a quantitative rock-property describing the reservoir. Therefore, seismic data are more uncertain than production data: it is pointless to try to match exactly each cell of a seimic impedance cube as is done with a least square comparison. Let us illustrate this fact with a simple example. In Figure 2, we display three seismic maps corresponding to a steam injection scenario in a heavy oil reservoir. The map on the left is the reference data to be matched and shows the growth of a steam chamber. The first simulated map displayed in Figure 2, middle, is the one obtained with an initial model before history matching. The last image on the left corresponds to a scenario without steam injection. Visually, the initial model is much closer to the reference data than the model without injection. Indeed, in this case the steam chamber is reproduced by simulation. However, the value of the objective function computed with the least square formulation between the reference data and the data produced by the initial model is higher (about 341) than the misfit calculated between the reference and the same model without injection (about 120). This example clearly illustrates that the formulation with the least square method doest not characterize the error between two seismic inverted data.

Recently, Tillier et al. [24] proposed to replace the least square formulation with a new measure based on image analysis tools. First, reference and simulated seismic data are filtered and clustered in order to extract the relevant information from the images. Then, these simplified images are compared with a modified local Hausdorff distance in order to capture spatial differences. Finally, the total error is computed as the euclidean norm of the Hausdorff distances. They show that this procedure yields a misfit measure which is able to discriminate seismic maps very efficiently on several reservoir cases [24], [25]. However, this new formulation consists of very elementary tools. The filtering step calls for a simple median filter, while the classification step is performed with the k-means algorithm, which does not account for spatial correlations in the image.

In this paper, we go one step further by proposing state-of-the-art methods for both the filtering and clustering steps. On the one hand, we investigate the potential of the NL means filter, which was shown to perform very well on several examples [6]. Its efficiency still has to be studied in the context of seismic data. On the other hand, we focus on segmentation methods based on active contours without edges [11] in order to replace the k-means algorithm. Since segmentation

methods use spatial information to detect shapes inside an image, they are expected to behave better than simple clustering. In the context of 4D seismic maps, we will generally extract two or three regions of interest. As a result, we extend the modified local Hausdorff distance to deal with more than two levels, in order to compare images with three target areas. The paper is organized as follows. In section 2, we first describe the new objective function and study the impact of the new NL-means filtering and segmentation steps on the procedure. Section 3 is dedicated to a synthetic resevoir case. We illustrate the potential of this new formulation with respect to the least square approach.

2. Objective function adapted to 4D seismic data: simplification and dissimilarities of images

In this paper, according to the meshing of the reservoir, we choose to divide the three dimensional seismic map into several two dimensional seismic slices and consider each slice as an image.
Since a seismic map contains a lot of information, we propose to first extract the most relevant information and focus on it. Then, the following step is to use an appropriate metric to measure the error between the relevant information derived from real seismic attributes and the one derived from the numerical outputs. The proposed formulation then consists of the three following steps:

1. Simplify images to extract the relevant information by filtering and segmentation. This process will be applied on both observed and simulated 4D seismic images.
2. Measure a local dissimilarity between the two simplified images.
3. Define a global dissimilarity to include it into the objective function.

In what follows, we will first study the NL-means filter [6] and a variational segmentation technique [9]. These tools will provide an efficient simplification step. Then, we adapt the local modified Haussdorff distance which was already proposed for step 2 by Tillier et al. [24]. In order to account for more than two regions of interest, we use the distance transform for real values proposed by Molchanov and Terán [20]. Finally, step 3 will only consist in computing the L2 norm of the local Haussdorff distances and will not be detailed here.

2.1. Simplification of seismic attributes with filtering and image segmentation

2.1.1. Preliminary step: Smoothing images.

As mentioned in the introduction, inverted seismic attributes are noisy and are also tainted by uncertainty due to the inversion process. Moreover, simulated seismic maps can also exhibit small patterns which are somewhat irrelevant and difficult to interpret. In order to prepare the segmentation step, we thus propose to clean up the data by filtering them.
The aim of filtering methods is to find the best estimation of an original image from its noisy version. A filtering method is based on the following decomposition:

$$u = D_h(u) + n(D_h, u) \tag{1}$$

where u is the noisy image, $D_h(u)$ is the estimated image, $n(D_h, u)$ is the estimated noise affecting the data and h is a filtering parameter. Among the several available local methods, some are based on local smoothing filters (arithmetic average filter, Gaussian filter, median filter or filter based

on calculus of variations [23]). For example, the arithmetic average filter replaces the value of one pixel by an arithmetic average of its neighboring cells or patch, the size of the patch being the parameter of the filter. Although computationally efficient, this filter is known to have serious difficulties at preserving contours. The use of the median filter, which replaces the value of each pixel by the median average value of its patch, makes it possible to lessen this effect. However, a large amount of noise can not be removed by the median filter. Local filters generally share this drawback.
Other filters worth mentioning call for thresholding techniques (Wiener-Fourier filter, Yaroslavsky local adaptive DCT-based filters [26] or wavelet thresholding method [13]). Recently, Buades et al. [6] introduced an efficient smoothing method known as the Non Local means filter (NL means filter). The main idea, first used by Efros and Leung [14] for texture synthesis, is to take advantage of self-similarities in images by comparing local neighbourhoods across the whole image. In the case of 4D inverted seismic images, this approach seems to be promising: seismic images are not structured such as natural pictures and consist of geological patterns or fluid displacement over large areas of the image. Coming back to equation (1), the NL means estimate of the denoised image is given by

$$D_h(u_0) = \frac{\sum_{y\in I} \exp\{-\frac{\|U(x)-U(y)\|}{2h}\}u(y)}{\sum_{y\in I} \exp\{-\frac{\|U(x)-U(y)\|}{2h}\}} \tag{2}$$

where $U(x)$ and $U(y)$ are the neighborhood windows, or patches, with respectively x and y as the central pixel. The distance between two patches is:

$$\|U(x) - U(y)\| = \frac{1}{s} \sum_{|j|\leq \frac{s-1}{2}} |u(x+i) - u(y+i)| \tag{3}$$

where s is the size of patches. In practice, the filtering parameter h depends on the noise variance of the image. This variance is unknown for a real picture u, but a possible estimation is given by the empirical variance

$$\sigma^2(u) = \frac{1}{|\ I\ |} \sum_{x\in I} (u(x) - \overline{u})^2$$

where I is the set of all pixels of u and $\overline{u} = \frac{1}{|I|} \sum_{x\in I} u(i)$.

In order to investigate the behavior of the NL means filter on seismic images, we propose to compare it with the arithmetic average and the median filter, which were already studied in this setting by Tillier et al. [24]. In both examples we set the filtering parameter h to 0.03 and the size of the patch to 7.

The first illustrative example deals with the steam chamber reservoir model presented in the introduction. The noisy image is depicted in Figure 4, top left. Results obtained with the three filters are given in the top row. As expected, the moving average filter exhibits over-smoothing, hence producing a blurred image, while the median filter makes it possible to preserve the steam chamber contours. The NL means filter (Figure 4 - line 1 column 3) also keeps intact the contours. In addition, we provide in Figure 4, bottom row, the noise removed by each filter, *i.e.* the difference between the noisy image and its denoised version. The image structure can be observed in the noise removed by the arithmetic average filter, this explains why a lot of information is lost in this case. On the contrary, the median filter removes a very small amount

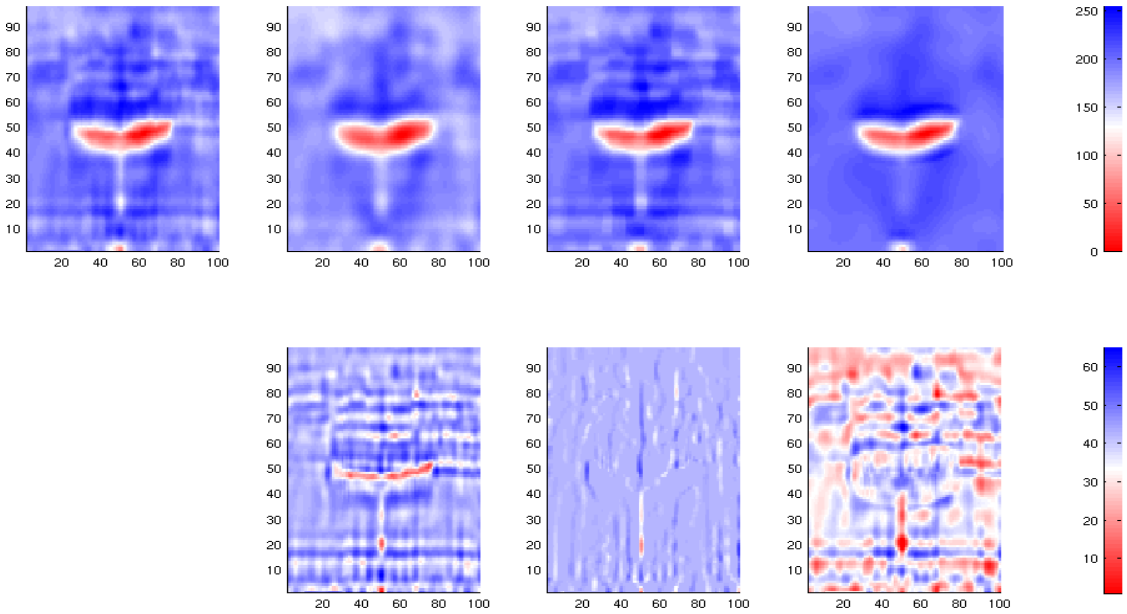

Figure 3: Comparison of three filters on a steam chamber reservoir case. First row: reference and filtered maps. Second row: noise removal. From left to right: reference, arithmetic average filter, median filter and NL means filter.

of noise: structural information is preserved, but small irrelevant patterns are not cut off. Between these two unwanted behaviors, the NL means filter produces a very clean image, where almost all the noise has been removed while preserving the steam chamber.

The second example focuses on a reservoir model encompassing several channels, *i.e.* geological structures which are preferential ways for fluid-flow displacement. Here, objects are numerous and contours have to be identified correctly since connectivity between channels is crucial for fluid displacements. On the top left part of Figure 4, the reference image consists of a noisy version of a synthetic seismic image. The initial map, containing normalized values between 0 and 1, has been corrupted with a Gaussian white noise with standard deviation equal to 0.03. Red areas correspond to channels with gas displacement and blue areas to channels with water displacement. Once again, the arithmetic average filter over-smooths the channel objects, and a lot of structural and connexity information is lost, as can be seen in the removed noise. Channels are less blurred with the median filter, but many details are removed in the red diagonal part of the image. Finally, the noise removed by the NL means filter looks like a white noise and the channel structure is very well preserved.

These reservoir examples clearly illustrate the large improvement provided by the NL means filter in the seismic data framework. This is the reason why we propose to include it into our objective function formulation. From a computational perspective, let us mention that Buades et al. advise to compute the weighted sum in equation (2) only on a subset of the image called the search window, in order to reduce CPU time. However, since relevant information (geological structures, fluid displacements) are observed on extensive areas of the image, we suggest to make this computation on the full image.

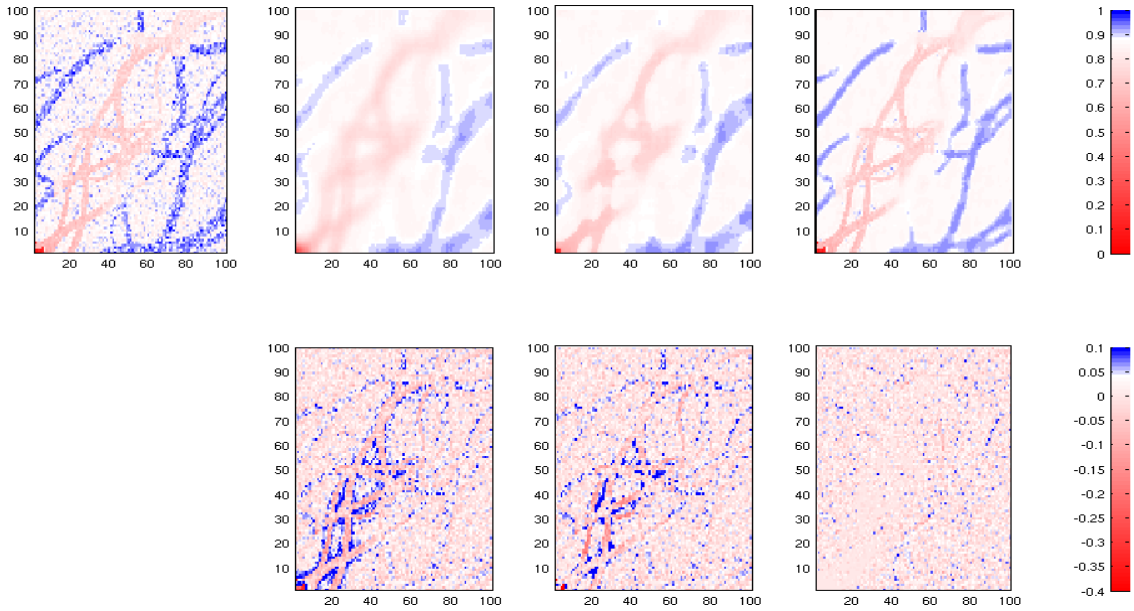

Figure 4: Comparison of three filters on a channelized reservoir case. First row: reference and filtered maps. Second row: noise removal. From left to right: reference, arithmetic average filter, median filter and NL means filter.

2.2. Segmentation

Seismic maps usually contain a lot of information. As mentioned before, in order to match the simulated map with the real data, we want to simplify both of them to only keep the main features. Consequently, the number of data will be significantly reduced to compare only the relevant information.

This step has to be done automatically without the operation of the user. Indeed, the history mathcing process usually involves hundreds of calls to the objective function during the iterations of the optimization algorithm. Previously in [24], statistical clustering methods such as the k-means algorithm have been tested for the simplification of the data. However, the proposed methods only deal with the absolute value of seismic attributes and do not incorporate information on structures and objects. Here, we propose to improve this clustering step by applying a segmentation based on variational methods, which accounts for spatial correlations in the image. In the image processing community, segmentation is the decomposition of an image into different areas of interest. For example, watersheds transform [5] is a basic tool of mathematical morphology for image segmentation. It is based on an analogy comparing images to topographic relief, where contours are defined as the water meeting points in a scenario of flood of the relief. This method uses the gradient of the image and can not be relevant when the edges in images are not well defined. Deformable models consist of algorithms which generate curves that move within images to find object boundaries by minimizing an energy function. Among the existing methods, active geodesic contours (Caselles et al. [7], [8]) and level set methods developed by Osher and Sethian [22] are the reference ones. Generally, they use an edge detector based on the gradient of the image.

In our case, even after applying a denoising method, the edges of the objects contained in the

seismic map are not accurate. As a result, gradient-based methods are not well suited for seismic maps. The active contours without edges proposed by Vese et al. ([9], [10], [11]) makes it possible to circumvent this limitation. This model uses a stopping term based on Mumford-Shah segmentation technique and has several advantages. First, it detects edges with and without gradient and second, the initial curve does not necessarily have to start around the objects to be detected and instead can be placed anywhere in the image. Then, it gives a partition of the image into two regions, the first region formed by the set of the detected objects and the second one consisting of the background. In our case, the objects to be detected can be for instance channels, steam chambers or any fluid displacement identified in the reservoir.
For illustration purposes, we first recall the reduced case introduced by Mumford and Shah [21]. Given a function u_0, which in the context of image segmentation is the image to be segmented, we are looking for its optimal piecewise-constant function approximation. This problem is called the "minimum partition problem". Mumford and Shah [21] propose to solve it by minimizing the following functional:

$$F^{MS}(K,u) = \sum_i \int_{\Omega_i} \mid u_0 - c_i \mid^2 + \mu \int_K d\mathcal{H}^1 \tag{4}$$

where $K = \cup_i \partial\Omega_i$ is a set of boundaries, $u = c_i$ inside each component Ω_i of $\Omega \backslash K$ and $\mathcal{H}^1$ is the one-dimensional Haussdorff measure. In two dimensions $\mathcal{H}^1$ is the length of the boundaries K. Generalization to three dimensions involves $\mathcal{H}^2$, the surface area of K. This energy is minimized with respect to the variable c_i by setting it to the mean of the image over Ω_i, *i.e.* $c_i = \frac{\int_{\Omega_i} u_0}{|\Omega_i|}$, where Ω_i represents a region where u is constant, and $\partial\Omega_i$ is the boundary of this region.

In order to minimize this energy over the set of piecewise-constant functions, Zhao et al. [27] propose to use a variational level-set approach. The unknown boundaries $\partial\Omega$ are represented by zero levels of a Lipschitz continuous function. Such a function $\phi : \Omega \to \mathbb{R}$ is used to divide the domain Ω in two open regions, defined respectively by $\{x \in \Omega, \phi(x) < 0\}$ and $\{x \in \Omega, \phi(x) > 0\}$. The edges of the objects to be identified in the image are then defined by $\{x \in \Omega, \phi(x) = 0\}$. Finally, the energy can be minimized with this following restriction:

$$\{u(x) = c_1 H(\phi(x)) + c_2 H(-\phi(x))\}$$

where H denotes the Heaviside function. Based on the Mumford-Shah equation, Chan and Vese [9] proposed a new model for active contours involving minimization of the following energy:

$$\begin{aligned} F(c_1, c_2, C) = \; & \lambda_1 \int_{\text{inside(C)}} (u_0(x,y) - c_1)^2 \, \text{dx dy} \\ & + \lambda_2 \int_{\text{outside(C)}} (u_0(x,y) - c_2)^2 \, \text{dx dy} \\ & + \mu \, \text{Length}(C) + \nu \, \text{Area}(C) \end{aligned} \tag{5}$$

where C is an evolving curve in Ω, $\mu > 0$ and $\nu > 0$ are regularization parameters and λ_1 and λ_2 are the weights assigned to each region.

Let us illustrate this model on the steam chamber example, where the object to be identified is precisely the steam chamber appearing in the middle of the image. Note first that the pixel values have to be positive in order to properly compute c_1 and c_2, the means inside our

target regions (steam chamber and the background). Consequently, original seimsic attributes are linearly mapped to grey level pixels between 0 and 255. In Figure 5, left, we recall the image obtained after NL means filtering. The result obtained after segmentation is given in Figure 5, right. Here, the steam chamber is clearly identified and separated from the non-informative background. Note also that the injection point at the bottom of the image is extracted.

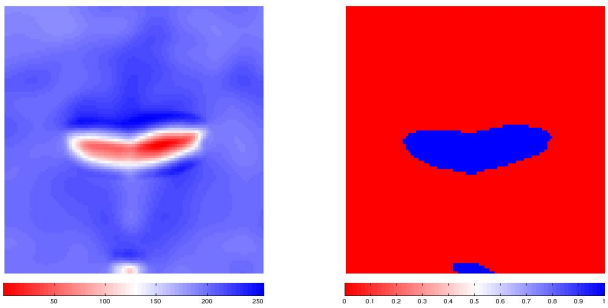

Figure 5: Chan and Vese segmentation on the steam chamber reservoir case. Left: Seismic map after NL means filtering. Right: Segmentation result (0: background, 1: detected object) with $\lambda_1 = 1$, $\lambda_2 = 4$, $\mu = 4500$, $\nu = 0$.

In this case, segmentation performs very well and makes it possible to extract the relevant information, *i.e.* the steam chamber growth. However, in general, 4D seismic images exhibit three types of impedance variations:

- regions with negative variations, which correspond to gas saturation or pressure increase (*e.g.* steam chamber in previous example);
- regions with positive variations, involving pressure decrease or water saturation increase;
- regions with almost zero variation, where there is no fluid displacement.

Direct application of the previous segmentation methodology will then fail at retrieving these three types of relevant regions. In order to represent more that two regions, a multiphase level-set was introduced by Chan and Vese [10], where several functions ϕ_i are used. Another generalization was proposed by Vese and Chung [11], where they use the idea of multilayer techniques for modeling epitaxial growth from [17] in order to represent several regions with fewer level-set functions. Here, we focus on this method and consider only one level-set function with an additional level. This model, which now divides the image into three regions, hinges upon the minimization of the following energy:

$$\begin{aligned} F(c_1, c_2, c_3, \phi) = & \int_\Omega \mid u_0(x) - c_1 \mid^2 H(-\phi(x))\, \mathrm{dx} \\ & + \int_\Omega \mid u_0(x) - c_2 \mid^2 H(\phi(x)) H(l - \phi)\, \mathrm{dx} \\ & + \int_\Omega \mid u_0(x) - c_3 \mid^2 H(\phi(x) - l)\, \mathrm{dx} \\ & + \mu \left[\int_\Omega \mid \nabla H(\phi) \mid + \int_\Omega \mid \nabla H(\phi(x) - l) \mid \right] \end{aligned} \tag{6}$$

where c_1, c_2 and c_3 are the means over each region and $\mu > 0$ is a regularization parameter. $\int_\Omega \mid \nabla H(\phi) \mid$ and $\int_\Omega \mid \nabla H(\phi(x) - l) \mid$ represent the length of the boundary between R_1,R_2 and R_2, R_3, respectively. The segmented image is finally given by:

$$u(x) = c_1 H(-\phi(x)) + c_2 H(\phi(x)) H(l - \phi(x)) + c_3 H(\phi(x) - l).$$

In order to write the associate Euler Lagrange equation and to minimize this energy with respect to the level-set function ϕ, the Heaviside function is approximated with a regularized version $H_\epsilon \in \mathrm{C}^1$. According to [9], we retain the following regularization of H:

$$H_\epsilon(x) = \frac{1}{2}\left(1 + \frac{1}{\pi}\,\mathrm{atan}\left(\frac{x}{\epsilon}\right)\right)$$

and its derivative is given by:

$$\delta_\epsilon(x) = H'_\epsilon = \frac{1}{\pi}\frac{\epsilon}{\epsilon^2 + x^2}.$$

Minimizing the regularized energy with respect to ϕ, c_1, c_2 and c_3 yields the associated Euler-Lagrange equations, where the descent direction is parameterized by an artificial time $t \geq 0$:

$$\begin{aligned}
\phi(0, x) =& \phi_0(x) \\
c_1(t) =& \frac{\int_\Omega u_0(x) H_\epsilon(-\phi(t, x))\,\mathrm{dx}}{\int_\Omega H(-\phi(t, x))\,\mathrm{dx}}, \\
c_2(t) =& \frac{\int_\Omega u_0(x) H_\epsilon(\phi(t, x)) H(l - \phi(t, x))\,\mathrm{dx}}{\int_\Omega H(\phi(t, x)) H(l - \phi(t, x))\,\mathrm{dx}}, \\
c_3(t) =& \frac{\int_\Omega u_0(x) H_\epsilon(\phi(t, x) - l)\,\mathrm{dx}}{\int_\Omega H_\epsilon(\phi(t, x) - l)\,\mathrm{dx}}, \\
\frac{\partial \phi}{\partial t} =& \delta_\epsilon(\phi)\left[\mid u_0 - c_1 \mid^2 - \mid u_0 - c_2 \mid^2 H_\epsilon(l - \phi) + \mu\,\mathrm{div}\left(\frac{\nabla \phi}{\mid \nabla \phi \mid}\right)\right] \\
&+ \delta_\epsilon(\phi - l)\left[H_\epsilon(\phi) \mid u_0 - c_2 \mid^2 - \mid u_0 - c_3 \mid^2 + \mu\,\mathrm{div}\left(\frac{\nabla \phi}{\mid \nabla \phi \mid}\right)\right], \\
&\frac{(\delta_\epsilon(\phi) + \delta_\epsilon(\phi - l))\nabla \phi}{\mid \nabla \phi \mid}.\vec{n} = 0 \ \text{ on } \delta\Omega, \ t > 0.
\end{aligned} \tag{7}$$

Here, $\vec{n}$ is the exterior unit normal to $\delta\Omega$. This energy is not convex; there is no guaranty to find the optimal minimizer.

With this new formulation for segmentation on three regions, we can now investigate its efficiency on the channelized reservoir already presented. In this example, positive variations correspond to gas displacement and negative ones to water movement. As in the steam chamber example, some pre-treatment of the data is required for efficient computation of the means over regions. The linear mapping proposed before is no longer suited, as positive and negative variations do not share the same order of magnitude. Here, a fair balance between positive and negative regions is achieved through histogram equalization [1]: original data are transformed so as to be distributed as close as possible to the uniform distribution on $[0, 255]$. The seismic image after NL means filtering and histogram equalization is given in Figure 6, left. The corresponding image after three-class segmentation is depicted in Figure 6, right. The regions identified by segmentation perfectly correspond to the expected areas, meaning that all fluid displacements are correctly extracted from the orginal seismic map.

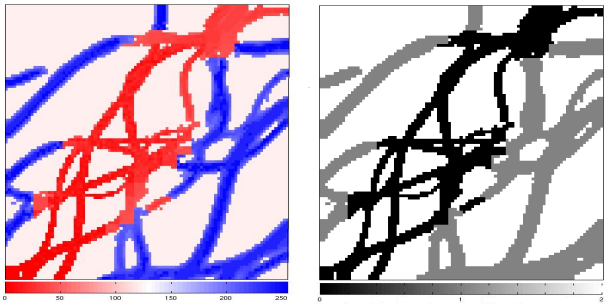

Figure 6: Multilayer level set segmentation on the channelized reservoir case. Left: Seismic map after NL means filtering and histogram equalization. Right: Segmentation result (0: first detected region, 1: second detected region, 2: background).

2.3. Image comparison and computation of the objective function

In the context of history matching, the previous segmentation step yields two segmented images in two or three regions: one for the reference 4D inverted seismic image and one for the image simulated by the reservoir model. Now, the goal is to establish the differences between these two simplified images and compute an objective function characterizing their mismatch. In a previous work [24], a computation of a Local Dissimilarity Map (LDM) has been efficiently used to compare two binary images. We extend here this formulation to three classes. In this section, we first recall the main ingredients to compute the LDM between two binary images. Then, we extend this method to compute the difference between images encompassing three classes. A global dissimilarities index is finally computed to obtain the value of the objective function between two images.

2.3.1. Local Dissimilarity Map

The Haussdorff distance is known to have an efficient application in image matching [12] or face recognition [18]. Given two non-empty sets of points $\mathbf{A} = (a_1, ..., a_n) \in \mathbb{R}^2$, $\mathbf{B} = (b_1, ..., b_n) \in \mathbb{R}^2$ and an underlying distance d, the Hausdorff distance between $\mathbf{A}$ and $\mathbf{B}$ is given by

$$D_H(\mathbf{A}, \mathbf{B}) = \max(h(\mathbf{A}, \mathbf{B}), h(\mathbf{B}, \mathbf{A}))$$

where $h(\mathbf{A}, \mathbf{B}) = \max_{a \in \mathbf{A}}(\min_{b \in \mathbf{B}} d(a, b))$. In image processing applications, this distance can be viewed as a dissimilarity measure between two binary images A and B. The Hausdorff distance has good properties, but it is quite sensitive to noise since it accounts for the most distant points in A and B. Several modifications of the Hausdorff distance have been proposed to improve it. The interested reader is referred to Zhao [28] for some overview of these modified distances. However, all of them are global and do not take into account local dissimilarities. To consider such a local aspect, Baudrier et al. [4] introduced the local dissimilarity map (LDM), which compares the two images locally through a sliding window centered on each considered pixel. The authors also propose a criterion to determine, for each pixel, the optimal size of the window. Practically, the LDM has an efficient formulation through the so-called distance transform. The distance transform of a given set associates to every point its distance to the nearest point in this set. More precisely, for binary images, the distance transform at one pixel is the distance between this pixel and the nearest black pixel (if the white color is the background and the black

color is the information of the binary image). Any metric could be used to measure the distance between two points, the most classical choice being the Euclidean distance. Using this distance transform, the LDM between two binary images A and B, at a pixel x, is given by

$$LDM_{A,B}(x) =\mid A(x) - B(x) \mid \max(\mathrm{dt}_A(x), \mathrm{dt}_B(x)) \tag{8}$$

where $dt_A(x)$ and $dt_B(x)$ are the distance transform of image A and B at pixel x, respectively. For binary images, this expression rewrites as follows:

$$LDM_{A,B}(x) = A(x)\mathrm{dt}_A(x) + B(x)\mathrm{dt}_B(x).$$

The definition of the LDM (8) can be directly applied to grey level images. However, while the definition of the distance transform is unique for binary images, this is no longer the case when dealing with grey level ones. Extensions of the distance transform for grey images are either achieved through an extended concept of distance between pixels, or with a new background definition. The grey-weighted distance transform and the weighted distance transform on curve space are two examples of such distance transform extending distances between pixels. Both distances are studied by Fouard and Gedda [15]. Besides, an approach based on an extension of the concept of background is proposed by Arlandis [2]. Here, we focus on the distance transform for real-valued functions proposed by Molchanov and Terán [20]. The main idea is to consider a grey level image I defined on $\mathbb{R}^2$ as a binary volume defined on $\mathbb{R}^2 \times \mathbb{R}$. Introduction of this additional dimension leads to the definition of the hypograph of image I given by:

$$\mathrm{hypo\,I} = \{(x, t) \in \mathbb{R}^2, I(x) \geq t\}.$$

This set consists of binary images obtained with all possible thresholds applied to image I. The original distance transform is then computed for each binary image included in hypo I, and the new distance transform is finally given by their weighted sum over the hypograph. For instance, if I encompasses grey level pixels in $[0, 1]$, the ν-weighted distance transform is defined as follows:

$$\bar{\mathrm{d}}(x, \mathrm{I}) = \int_{\inf \mathrm{I}}^{\sup I} \mathrm{d}(x, \mathcal{I}_t)\nu(\mathrm{dt})$$

where ν is a finite measure on $[0, 1]$ and $\mathcal{I}_t = \{x \in \mathbb{R}^2, \mathrm{I} \geq t\}$. Similarly, if I is discretized on $[0, 255]$ and has values between a and b, the ν-weighted distance transform becomes:

$$\bar{\mathrm{d}}(x, \mathrm{I}) = \frac{1}{255} \sum_{i=a}^{b} \mathrm{d}(x, \mathcal{I}_i)w_i$$

for some weights w_i. In both formulations above, d is a distance between a point and a set, classically given by $\mathrm{d}(x, F) = \inf\{\rho(x, y), y \in F\}$ for some point x and a set F. Here, ρ is chosen as the Euclidean distance, but any distance could be used. This new distance transform is then used in equation (8) to compute the LDM between the simulated and the reference segmented images.
Finally, the LDM is summarized in a scalar objective function through L2-norm averaging.

2.4. Summary

Finally, the new formulation adapted to 4D seismic data consists of the following steps:

1. Apply the NL means filter on real seismic attributes and the ones derived from the responses of the given reservoir model.
2. Extract relevant information from both maps using
   - Chan and Vese segmentation method [9] for two regions
   - Vese and Chung segmentation method [11] for three regions

   Note that preliminary transformation of the data may be needed before segmentation (linear mapping, histogram equalization).
3. Compute the LDM between the segmented images with the appropriate distance transform (depending on the number of classes).
4. The final scalar objective function is obtained by computing the L2 norm of the LDM.

3. Application on an history matching case

4. Conclusion

[1] T. Acharya and A.K. Ray, *Image Processing: Principles and Applications.*, Wiley-Interscience, 2005.
[2] J. Arlandis, J. C. Prez-Cortes, and R. Llobet, *Handwritten Character Recognition using the Continuous Distance Transformation*, in ICPR, 2000, pp. 1940-1943.
[3] K. Aziz and A. Settari, *Petroleum reservoir simulation*, Applied Science Publishers, 1979.
[4] E. Baudrier, F. Nicolier, G. Millon, and S. Ruan, *The Adaptative Local Hausdorff-Distance Map as a new Dissimilarity Measure*, Pattern Recognition, vol. 41, iss. 5, pp. 1461-1478, 2008.
[5] S. Beucher, *The watershed transformation applied to image segmentation.*, 10th Pfefferkorn Conference on Signal and Image Processing in Microscopy and Microanalysis, 16-19 Sept 2011.
[6] A. Buades, B. Coll et J. M. Morel, *A Review of Image Denoising Algorithms, with a New One*, Society for Industrial and Applied Mathematics, 2005.
[7] V. Caselles, R. Kimmel, and G. Sapiro, *Geodesic Active Contours*. International Journal of computer Vision, 22(1):6187, 1993.
[8] V. Caselles, F. Catt, C. Coll, and F. Dibos, *A geometric model for active contours in image processing*, Numerische Mathematik., 66:131, 1993.
[9] T. Chan and L. Vese, *Active Contours Without Edges*, IEEE Transactions on image Processing, 2001.
[10] T. Chan and L. Vese, *A Multiphase Level Set Framework for Image Segmentation Using the Mumford and Shah Model*, International Journal of Computer Vision, 2002.
[11] G. Chung and L. Vese, *Energy Minimization Based Segmentation and Denoising Using a Multilayer Level Set Approach*, Computer Vision and Pattern Recognition: 5th International Workshop, 2005.
[12] M-P. Dubuissonand A. K. Jain, *A Modiffed Hausdorff Distance for Object Matching*, Proc. International Conference on Pattern Recognition, pp 566-588, 1994.
[13] D. Donoho and I. Johnstone, *Ideal spatial adaptation via wavelet shrinkage*, Biometrika, 81 (1994), pp. 425–455.
[14] A. Efros and T. Leung, *Texture synthesis by non parametric sampling*, In Proc. Int. Conf. Computer Vision, volume 2, pages 10331038, 1999.
[15] C. Fouard and M. Gedda, *An Objective Comparison between Gray Weighted Distance Transforms and Weighted Distance Transforms On Curved Spaces*, in Proc. of DGCI'06, 2006.
[16] O. Gosselin, S.I. Aanonsen, I. Aavastamark, A. Cominelli, R. Gonard,M. Kolasinski,F. Ferdinandi, L. Kovacic and K. Neylon, *History Matching Using Time-lapse Seismic (HUTS)*, SPE 84464, SPE Annual Technical conference and Exhibition, Denver, Colorado, U.S.A., 2003.
[17] M.F. Gyure, C. Ratsch, B. Merriman, R.E. Caflisch, S. Osch, J.J. Zinck, D.D. Vvedensky, *Level-set methods for the simulation of epitaxial phenomena*, Physical Raview E 58(6): R6927-R6930 Part A, 1998
[18] O. Jesorsky, K. J. Kirchberg and R. W. Frischholz, *Robust Face Detection Using the Hausdorff Distance*, In Proc. Third International Conference on Audio- and Video-based Biometric Person Authentication, Springer, Lecture Notes in Computer Science, LNCS-2091, pp. 9095, Halmstad, Sweden, 68 June 2001.
[19] R.D. Mindlin, *Compliance of elastic bodies in contact*, J. Appl. Mech., 16 (1949), pp. 259268.
[20] I. S. Molchanov and P. Terán, *Distance transforms for real-valued functions*, J. Math. Anal. Appl., iss. 278, pp. 472-484, 2003.
[21] D. Mumford and J. Shah, *Optimal approximation by piecewise smooth functions and associed variational problems*, Commun. Pure Appl. Math, 1989.
[22] S. Osher and J.A. Sethian, *Fronts propagation with curvature dependent speed : Algorithms based on Hamilton-Jacobi formulations.*, Journal of Computational Physics, 79,1988.
[23] L. Rudin and S. Osher, *Total variation based image restoration with free local constraints, in Proceedings of the IEEE International Conference on Image Processing*, Vol. 1, Austin, TX, 1994, pp. 31–35.
[24] E. Tillier, S. Da Veiga and R. Derfoul, *Appropriate formulation of the objective function for the history matching of seismic attributes.*, submitted to Computers and Geosciences.
[25] E. Tillier, M. Le Ravalec and S. Da Veiga, *Simultaneous inversion of production data and seismic attributes: Application to a SAGD produced field*, Oil Gas Science Tech., to be published.
[26] L. P. Yaroslavsky, *Digital Picture Processing. An Introduction*, Springer-Verlag, Berlin, 1985.
[27] H.-K. Zhao, T. Chan, B. Merriman, and S. Osher, *Variational level set approach to multiphase motion*, JCP 127(1): 179-195, 1996.
[28] C. Zhao, W. Shi and Y. Deng, *A new Hausdorff distance for image matching*, Pattern Recognition Letters, vol. 26, no 5, 2005, pp. 581-586.